



Swansea University
Prifysgol Abertawe



Cronfa - Swansea University Open Access Repository

This is an author produced version of a paper published in :

Meccanica

Cronfa URL for this paper:

<http://cronfa.swan.ac.uk/Record/cronfa31985>

Paper:

Vijayan, K., Vljajic, N. & Friswell, M. (2017). Drillstring-borehole interaction: backward whirl instabilities and axial loading. *Meccanica*

<http://dx.doi.org/10.1007/s11012-017-0623-3>

This article is brought to you by Swansea University. Any person downloading material is agreeing to abide by the terms of the repository licence. Authors are personally responsible for adhering to publisher restrictions or conditions. When uploading content they are required to comply with their publisher agreement and the SHERPA RoMEO database to judge whether or not it is copyright safe to add this version of the paper to this repository.

<http://www.swansea.ac.uk/iss/researchsupport/cronfa-support/>

Drillstring-borehole interaction: backward whirl instabilities and axial loading

K.Vijayan · N. Vljajic · M.I. Friswell

Received: date / Accepted: date

Abstract A major concern within the oil drilling industry remains the high risk associated with the drilling bit and tool failure from the build-up of damaging vibrations. Effective understanding of the drillstring dynamics is essential for efficient drilling operation. Complex dynamic behaviour is often observed in the drillstring due to friction, impact, unbalance eccentricity and energy exchange between different modes of vibrations. The interaction between the drillstring and borehole wall involves nonlinearities in the form of friction and contact. Initially a two discs model was developed to analyse the behaviour of the system. The theoretical model was tuned by altering the phase of the eccentric mass. This excites each lateral modes of the system in isolation. The effects of impact, friction and mass unbalance are included in the model. The drillstring borehole interaction induces whirling behaviour of the drillstring causing forward whirl, backward whirl or intermittent bouncing behaviour depending on the system parameters. A critical steady state behaviour within the system is the backward whirling of the drillstring, which reduces the fatigue life of the drillstring. For the tuned system the backward whirl behaviour was analysed by carrying out a rotor speed sweep spanning the lateral natural frequencies. The influence of rotor speed on the system dynamics is explored using a run up and run down and is analysed using a waterfall plot. The waterfall plot indicated the frequency of maximum response corresponding to each

K.Vijayan

Department of Ocean engineering and Naval architecture, Indian Institute of Technology Kharagpur, Kharagpur 721302, India Tel.: +91-3222-281782

Fax: +91-3222-282284

E-mail: kiran.vijayan@gmail.com

N. Vljajic

Department of Engineering Mathematics, University of Bristol, Queen's Building, Bristol BS8 1TR, UK

M.I. Friswell

College of Engineering, Swansea University, Singleton Park, Swansea, SA2 8PP, UK

rotor speed. Depending on the whirling behaviour the dominant frequency was observed at the lateral natural frequency, the rotational speed or the backward whirl frequency. The influence of variation in whirling behaviour due to altering of the axial load was analysed for a multiple disc case consisting of five discs. A transition in behaviour along the length of the drillstring was observed due to the axial load and bending moment interactions. Depending on the mode excited impact and sustained contact initiation with the borehole varied across the different stabilizer locations.

Keywords Rotor dynamics · drill string · backward whirl

1 Introduction

During extraction of petroleum and natural resources, boreholes that run many kilometres are created using drillstrings. Drillstrings are long slender structures which are made up of three sections namely, the drill pipe, the drill collar and a drill bit. The purpose of the drill pipe is to transmit torque to the bit. The drill collar is heavier in weight per unit length than drill pipe provides the compressive load on the drill bit. The combination of the drill bit and drill collar is called the bottom hole assembly (BHA). A major concern in the oil drilling industry is the high cost and lead time caused due to the drillstring and bit failure from the build up of damaging vibration.

A combination of torsional, axial and lateral vibration exist along the drillstring. The length of the drill assembly increases the possibility of energy exchange between various modes of vibrations. Drilling vibration may lead to poor efficiency of the process, excessive wear at the tools or fracture of the drilling system. The four main problems originating from this are drill pipe fatigue, drillstring component failure, well bore instability and bit damage. The causes of vibration include impact and friction at the borehole/drill string and bit formation interfaces, unbalance eccentricity or initial curvature in drill collar sections and energy exchange between various modes of vibration.

Among the different vibrations lateral vibrations which usually result in whirling behaviour within the drillstring however can be the most destructive. The rotating stabilizer hitting the rock formation can send shocks through the collars [1, 2] which can be as high as 250g [3]. If the shaft has one or more rotors attached, more complicated whirl phenomena can occur. Field studies [4] indicate that if a rotating drillbit is suddenly arrested, rapid whirling of the drillstring can occur.

Various authors [5, 6, 7, 8, 9, 10, 11, 12, 13] have described the non-linear phenomena that characterize similar phenomenon within the context of rotor dynamics. Whirling of a shaft or rotor can result in rubbing/interaction with the enclosure or bearing. Problems of rubbing involve investigation of two main effects: determination of local casing rotor interaction and the global vibration of the rotor casing/bearing. The frequencies present in the measured vibration signal constitute some of the most useful information for diagnosing rotor dynamics problems.

Basically there are two common steady state vibration regimes of rotor motion which are created by rub. These steady states are usually reached through some transient motions involving partially rubbing surfaces. The first steady state regime is due to unbalance and the second is a self excited vibration. The former is less dangerous but the latter can often cause catastrophic failure. Steady state whirl due to unbalance usually occurs during transient conditions of start-up and/or shutdowns when the rotor passes through the resonance speed. This regime is often referred as full annular rub. The second of the quasi stable steady state regimes, which could be more serious in its destructive effect, is the self excited backward full annular rub known as “backward whirl.”

One of the simplest models that can be used to study the flexural behaviour of rotors consists of a point mass attached to a massless flexible shaft. This model is often referred to as the Jeffcott rotor [11, 14]. Several authors have tried to formulate the equations of motion in polar [10, 15] and Cartesian coordinates [6, 16].

One of the key parameters during manufacturing is the eccentricity associated with the disc. Even with a fine manufacturing tolerance mass eccentricity is bound to be present in most of the system. Previous studies have not explored the influence of an individual mode excited in isolation on the backward whirl behaviour. Backward whirl is critical since it affects the fatigue life of the drillstring. For the present study the location and mass of the eccentricity will be carefully tuned to excite each modes of the system in isolation. Initially the study will be carried out on a two disc model. A similar instability study using an experimental set-up consisting of two discs vertically connected using a string was carried out by Mihajlovic et al. [17, 18]. The location of each disc represents the stabilizer location on the drillstring. This model will be extended to a multiple disc system in order to incorporate the influence of axial loading/self weight on the whirling behaviour of the multiple disc system.

2 Modelling of a coupled two disc model

Initially the study was carried out on a model with two two disc attached on a massless shaft as shown in Fig. 1. The rotor disc with eccentric masses were coupled using spring elements. Each disc is modelled as a lumped mass located eccentrically rotating at rotor speed ω . In the model one end of the rotor is attached to the drive and the other represents the free end of the drillstring which is modelled by altering the torsional stiffness. The mass located eccentrically rotates at rotor speed ω as shown in Fig. 2. The rotor is displaced from the geometric center of the “borehole” by a distance (δ) and a linear spring of stiffness \mathbf{k}_1 is used to model the restoring force which is due to the bending of the shaft. The angular position of the shaft centre is denoted by θ_i . The position vector of the shaft centre and eccentric mass R_{iM} and R_{im} are given

by

$$R_{iM} = x_i \hat{i} + y_i \hat{j} \quad (1)$$

$$R_{im} = [x_i + e_i \cos(\Psi + \theta_i + \phi_i)] \hat{i} + [y_i + e_i \sin(\Psi + \theta_i + \phi_i)] \hat{j} \quad (2)$$

where (x_i, y_i) is the position of the shaft centre for disc i , e_i is the position of the eccentric mass with respect to the shaft centre, θ_i is the torsion angle of the disc i , ψ is the rotational angle of the drive which for a constant rotational speed (ω) will be ωt and ϕ_i is the phase angle of the eccentric mass.

The kinetic energy (T) of the system is given as

$$T = \frac{1}{2} \sum_{i=1}^2 M_i \dot{R}_{iM}^2 + J_i (\dot{\Psi} + \dot{\theta}_i)^2 + m_i \dot{R}_{im}^2 \quad (3)$$

where M_i is the mass of disc i and m_i is the eccentric mass of disc i . J_i is the polar moment of inertia of disc i . The potential energy (V) of the system is

$$V = \frac{k_1}{2} (x_1^2 + y_1^2) + \frac{k_2}{2} (x_2^2 + y_2^2) + \frac{k_c}{2} (x_2 - x_1)^2 + \frac{k_c}{2} (y_2 - y_1)^2 + \frac{k_t}{2} (\theta_1)^2 + \frac{k_{tc}}{2} (\theta_2 - \theta_1)^2 \quad (4)$$

where k_1, k_2 are the first and the second rotor stiffness to the ground in the X and Y directions respectively. k_c is the coupling stiffness between the two rotor discs in the X and Y directions. The system is modelled symmetrically with stiffness identical in the X and Y directions. k_t and k_{tc} are the torsional stiffness and torsional coupling stiffness respectively of the shaft. Using the Lagrange formulation the equations of motion are formulated in the X, Y and θ directions as

$$\frac{d}{dt} \left(\frac{\partial T}{\partial \dot{x}_i} \right) - \frac{\partial T}{\partial x_i} + \frac{\partial V}{\partial x_i} = F_{x(i)} \quad (5)$$

$$\frac{d}{dt} \left(\frac{\partial T}{\partial \dot{y}_i} \right) - \frac{\partial T}{\partial y_i} + \frac{\partial V}{\partial y_i} = F_{y(i)} \quad (6)$$

$$\frac{d}{dt} \left(\frac{\partial T}{\partial \dot{\theta}_i} \right) - \frac{\partial T}{\partial \theta_i} + \frac{\partial V}{\partial \theta_i} = M_{\theta(i)} \quad (7)$$

Substituting for the kinetic and potential expressions we obtain the undamped equation of motion. As shown in Fig. 2 damping was included in the lateral X and Y direction and torsional θ direction. The external excitation is provided from the unbalance eccentricity or initial curvature in drillstring sections. The external force and moment in the X, Y and θ direction is obtained as:

$$F_{x(i)} = m_i e_i [(\dot{\Psi} + \dot{\theta}_i)^2 \cos(\Psi + \theta_i + \phi_i)] \quad (8)$$

$$F_{y(i)} = m_i e_i [(\dot{\Psi} + \dot{\theta}_i)^2 \sin(\Psi + \theta_i + \phi_i)] \quad (9)$$

$$M_{\theta(i)} = m_i e_i [\ddot{x}_i \sin(\Psi + \theta_i + \phi_i) - \ddot{y}_i \cos(\Psi + \theta_i + \phi_i)] \quad (10)$$

Since the shaft is vertical gravitational force doesn't influence the lateral motions. Substituting the external force and moment and the damping terms the final equation of motion for the two disc rotor is obtained as:

$$\begin{aligned}
(M_1 + m_1)\ddot{x}_1 + c_1\dot{x}_1 + k_1x_1 + k_c(x_1 - x_2) &= m_1e_1[(\dot{\Psi} + \dot{\theta}_1)^2 \cos(\Psi + \theta_1 + \phi_1) \\
&\quad + (\ddot{\Psi} + \ddot{\theta}_1) \sin(\Psi + \theta_1 + \phi_1)] \\
(M_1 + m_1)\ddot{y}_1 + c_1\dot{y}_1 + k_1y_1 + k_c(y_1 - y_2) &= m_1e_1[(\dot{\Psi} + \dot{\theta}_1)^2 \sin(\Psi + \theta_1 + \phi_1) \\
&\quad - (\ddot{\Psi} + \ddot{\theta}_1) \cos(\Psi + \theta_1 + \phi_1)] \\
(J_1 + m_1e^2)\ddot{\theta}_1 + c_{t1}\dot{\theta}_1 + k_{t1}\theta_1 + k_{tc}(\theta_1 - \theta_2) &= m_1e_1[\dot{x}_1 \sin(\Psi + \theta_1 + \phi_1) \\
&\quad - \dot{y}_1 \cos(\Psi + \theta_1 + \phi_1)] \\
(M_2 + m_2)\ddot{x}_2 + c_2\dot{x}_2 + k_2x_2 + k_c(x_2 - x_1) &= m_2e_2[(\dot{\Psi} + \dot{\theta}_2)^2 \cos(\Psi + \theta_2 + \phi_2) \\
&\quad + (\ddot{\Psi} + \ddot{\theta}_2) \sin(\Psi + \theta_2 + \phi_2)] \\
(M_2 + m_2)\ddot{y}_2 + c_2\dot{y}_2 + k_2y_2 + k_c(y_2 - y_1) &= m_2e_2[(\dot{\Psi} + \dot{\theta}_2)^2 \sin(\Psi + \theta_2 + \phi_2) \\
&\quad - (\ddot{\Psi} + \ddot{\theta}_2) \cos(\Psi + \theta_2 + \phi_2)] \\
(J_2 + m_2e^2)\ddot{\theta}_2 + c_{t2}\dot{\theta}_2 + k_{t2}\theta_2 + k_{tc}(\theta_2 - \theta_1) &= m_2e_2[\dot{x}_2 \sin(\Psi + \theta_2 + \phi_2) \\
&\quad - \dot{y}_2 \cos(\Psi + \theta_2 + \phi_2)] \quad (11)
\end{aligned}$$

where c_1 and c_2 are the damping coefficients of first and second rotor discs.

2.1 Contact modelling

The next phenomenon that needs to be modelled is the effect of the contact between the borehole wall and the whirling drillstring especially at the stabilizer location. The expression without impact given in eq. (11) contains geometric non-linearities in the inertia terms due to coupling between the torsional and lateral motions. However a stronger non-linearity is induced due to impact and friction at the borehole/drill string and bit formation interfaces.

Similar to the impact of a rotor against a stator within the rotor-dynamic context the whirling drillstring can impact the borehole wall. In addition to the plastic deformation the contact between the system also causes dissipation due to the frictional force. There are a plethora of models available for friction. The present study is analysing the drillstring borehole interaction, not involving detailed analysis on the stick-slip or the drilling cutter behaviour. Hence for the present model the frictional force is assumed to be Coulomb [19, 20] with no Stribeck or viscous effect even though there is an uncertainty in the type of model to be used [10]. For numerical stability in the simulation, the variation in the friction coefficient with relative velocity (V_{rel}) was smoothed using a continuous function, such that

$$\mu = \mu_d \tanh\left(\frac{V_{rel}}{V_0}\right) \quad (12)$$

where μ_d is the dynamic friction coefficient, V_{rel} is the relative velocity at the contact interface given by

$$\begin{aligned} V_{\text{rel}}(i) &= (\dot{\Psi} + \dot{\theta}_i)R_i - \dot{x}_i \frac{y_i}{\rho_i} - \dot{y}_i \frac{x_i}{\rho_i} \\ &= (\dot{\Psi} + \dot{\theta}_i)R_i - \dot{x}_i \sin \alpha_i - \dot{y}_i \cos \alpha_i \end{aligned} \quad (13)$$

where $\rho_i = \sqrt{x_i^2 + y_i^2}$ and $\alpha_i = \arctan(\frac{y_i}{x_i})$. V_0 is a constant and its value can be varied to obtain different velocity profiles at the contact region. The model is a reasonable first approximation of the forces acting in the real system except that the effect of drilling mud influences the response in the form of fluid-structure interaction, which is neglected.

Contact with the borehole generates a normal force in the radial direction (F_n) and a frictional force in the tangential direction (F_t). Contact is modelled using a spring of relatively high stiffness. Damping is included in the model to incorporate the effect of a coefficient of restitution. The contact force generated in the radial direction is given by

$$\begin{aligned} F_{n(i)} &= k_s(\rho_i - \delta_i) + c_s \dot{\rho}_i & \text{for } \rho_i > \delta_i \\ &= 0 & \text{for } \rho_i \leq \delta_i \end{aligned} \quad (14)$$

where δ_i is the clearance. The frictional force is modelled using Coulomb friction which generates the tangential force ($F_{t(i)}$)

$$F_{t(i)} = \mu F_{n(i)} \quad (15)$$

Transforming the forces to Cartesian coordinates we obtain the forces in the X and Y directions as

$$\begin{aligned} F_{x(i)} &= -F_{t(i)} \sin \alpha - F_{n(i)} \cos \alpha \\ F_{y(i)} &= F_{t(i)} \cos \alpha - F_{n(i)} \sin \alpha \end{aligned} \quad (16)$$

The frictional moment generated in the torsional direction is:

$$M_{\text{ext}(i)} = R_i F_{t(i)} \quad (17)$$

These additional external forces and moments were incorporated in eq. (11) to obtain the expression for the equation of motion for the coupled two disc system with contact.

2.2 Results and discussion for the two disc model

Using the theoretical model the system was simulated for the parameters given in Table 1. Torsional damping is assumed to be small for the present study similar to rotor dynamic systems [19]. However within an actual drilling environment the torsional damping could be higher due to the drilling mud and formations. The natural frequencies of the system and the mode shapes are given in Table 2. For the given set of parameters the two lateral modes are

well separated in frequency. The coupling stiffness in the lateral direction was chosen higher than the stiffness to the ground since during whirling motion the system is generally supported by the coupling spring.

A case study by exciting each mode in isolation was carried out by altering the relative phase of the eccentric mass location. Initially the eccentric mass was located at the same angular position for both the discs. This implies that the external excitation forces due to unbalance acts in phase for both the discs, therefore exciting the first mode of the system. Since the initial condition is also important the rotor speed range was chosen to span near the first lateral natural frequencies of the system. A frequency sweep was carried out by varying the rotor speed during the forward sweep from 0.096 to 0.4 Hz. The speed was incremented by 0.0016 Hz after every 500 seconds. The temporal variations in the responses of both rotors are shown in Fig. 3. The duration and step size for the speed increment was chosen to reduce the initial transient in the response. In eq. (11) the speed increment also induces a phase change in the eccentricity force which induces artificial transients on the rotor disc during each speed increment. This artefact was corrected by incorporating a phase correction to compensate for the phase change during the speed increments. Figure 3 clearly indicates that the system establishes contact at nearly the same instant on both discs. For clarity only the run up is shown, during the run down test the drillstring is continuously in contact with the borehole.

A waterfall spectrum may be used to study the key response frequencies. A waterfall spectrum is a three dimensional frequency response spectrum corresponding to various rotational speeds. The frequency response was averaged by sampling across sections of the time series. The contour plot of averaged waterfall spectrum is shown in Fig. 4. The contour plot during the forward sweep shown in Fig. 4(a) indicates that the frequency corresponding to maximum response jumps when the rotor speed is near the lateral natural frequency of the system. The subsequent peaks are observed at $\frac{R}{\delta}\omega$ where ω is the rotor speed which corresponds to the backward whirl frequency with the drillstring rolling along the borehole surface. The averaged contour plot of the waterfall spectrum during reverse sweep is shown in Fig. 4(b). A hysteresis in the frequency content near the jump frequency was also observed. During run down the backward whirl frequency was persistent beyond the lateral frequency.

Next the initial position of the eccentric mass on the second rotor was altered to be 180 degree out of phase to that on the first rotor. This excites the second lateral mode and thus delays rotor speed at which continuous contact between the drillstring and borehole is established. Since the excitation force is dependent on the square of the rotor speed the starting speed for the sweeping was more offset from the second natural frequency at 0.72 Hz. The frequency sweeping was carried out from 0.57 to 0.96 Hz. For brevity the response of the system for the same sweeping range as the one used in exciting the first mode is not shown however the behaviour was as expected for a system with no contact established since the first mode is not excited. The variation in the temporal response is shown in Fig. 5 similar to Fig. 3 for

forward sweep. The jump in frequency content occurs when the rotor speed approaches the second lateral natural frequency of the system is observed in Fig. 6 which is hysteric similar to Fig 4 .

3 Modelling of drillstring

The study until now indicates that the position and phase of the eccentricity on the two discs influences the instant when the backward whirl is initiated. In practice the drilling operator alters the surface controlled drilling parameters, such as axial loading, drilling fluid flow through the drill pipe, the drillstring rotational speed and the density and viscosity of the drilling fluid to optimise the drilling operation. For the present study fluid modelling is not considered. In order to understand the behaviour of a long drillstring the two disc model has to be extended to a multiple disc which can be envisaged as the multiple stabilizer attached to the drillstring. For the multiple disc model the axial loading due to self weight is incorporated in the model.

The self weight causes the axial force to vary from tension along the drill pipe to compression on the drill collar. The location of the neutral point determines the static weight on bit. The drilling operator applies an axial load at the surface end called the hook load. This is a controllable parameter which the driller alters during the drilling operation to adjust the weight on bit (WOB). The WOB needs to be altered to prevent buckling of the drillstring [21]. This modifies the location of the neutral point along the drillstring. The drill pipe is generally in tension and the thicker drill collar is under compression. The net axial load at the bit arises from a combination of the axial load and gravity. The present study will consider the modification in the bending stiffness due to axial loading. The influence of the axial loading on the bending stiffness of the drillstring is bound to increase with increasing length of the drillstring. Generally a reduction in out of plane bending stiffness can be expected with increase in drillstring length.

The actual drillstring is asymmetric with the lighter drillpipe forming the upper section and heavier drill collar forming the bottom section which applies weight on the bit. The drillstring parameters [22] are given in Table 3. The density and the inner diameter was different for the drill collar as shown in Fig. 7. Drill collar material was chosen four times denser than the drill pipe and inner diameter was 0.5 times the inner diameter of the drill pipe. This creates a variation in the axial force along the drillstring. A finite element model was developed for the drillstring. The drillpipe and drill collar were modelled as an Euler- Beuroulli beam with 20 elements. The boundary condition was taken as pinned at the ends. The bending stiffness change for a 2 node Euler-Bernoulli beam of length l due to axial compression force (f_e) is given by [12, 23, 24]:

$$\mathbf{K}_{c(i)} = \frac{\mathbf{f}_e}{30\mathbf{l}} \begin{bmatrix} 36 & 3l & -36 & 3l \\ 3l & 4l^2 & -3l & -l^2 \\ -36 & -3l & 36 & -3l \\ 3l & -l^2 & -3l & 4l^2 \end{bmatrix} \quad (18)$$

Axial force across each individual coupled disc section will be the equilibrium force resulting from the hook load and the gravitational force. The net f_e in eq. (18) at the node was determined by averaging the axial load across the nodes of the element. A typical variation in the first five natural frequencies of the drillstring is shown in Fig. 8. Minimum hook load was chosen such that the first natural frequency is almost zero. Corresponding to the minimum hook load the lower section of the drillstring is in compression as shown in Fig. 9. The first natural frequency corresponds to the buckling mode. Increase in the hook load causes the antinode location to shift more towards the centre as shown in Fig. 10.

The finite element study provided an understanding on the influence of axial load on the natural frequency and the buckled mode shape of the drillstring. Using the minimum hook load a multiple disc system was modelled in order to excite the different modes of the system individually.

3.1 Modelling of multiple disc model

A lumped parameter model with five discs was chosen as a typical example. In contrast to the two disc system, in order to excite the different modes of the system both the mass and position of the eccentricity have to be altered simultaneously. As a typical example to excite the third mode of a five disc the position of the eccentric masses should be $\mathbf{e} = [1 \ 0 \ 1 \ 0 \ 1]$ and the particular combination of phase should be $\phi = [0 \ 0 \ \pi \ 0 \ 0]$.

A static condensation is carried out in eq. (18) treating the translational DOFs as master DOFs and the rotational DOFs as slave DOFs. The reduced stiffness matrix is then obtained as:

$$\mathbf{K}_{c(i)} = \frac{\mathbf{f}_e}{\mathbf{l}} \begin{bmatrix} 1 & -1 \\ -1 & 1 \end{bmatrix} \quad (19)$$

Compared to the finite element model of the drillstring with 20 elements the lumped model consists of five mass elements. Hence the hook load was chosen slightly higher than the minimum hook load obtained from the finite element model. A typical case study was carried out for a hook load of 3.5 MN. This induces compression at the bottom drillcollar section of the drillstring. The eccentricity mass position and phase were modified to initiate the system in the first mode. A frequency sweep study was carried out by varying the

rotor speed from 0.005 to 0.04 Hz with a step change of 0.005 Hz after every 500 seconds. Since the frequencies are small the damping in the lateral and torsional direction was chosen slightly higher. The step size, duration and damping was chosen to reduce the transients during the frequency sweep study. The frequency sweep range spans the first natural frequencies of the drillstring. The normalised temporal response shown in Fig. 11 indicates that the contact is not initiated at the same instant for all the discs. The disc which initiates the impact and sustained contact depends on the mode shape. This is correlated to the fact that higher deflection occurs at the drill collar section in the buckled state of the drillstring.

4 Conclusion

The behaviour of a rotor disc system considering the initiation of critical steady regimes such as backward whirl was analysed. The initial study on a two disc rotor identified different steady state regimes including backward whirl behaviour. Each mode of the coupled two disc model was excited in isolation by varying the initial phase difference between the eccentric masses of the two discs. This controlled the initiation of backward whirl or continuous contact between the drillstring and the borehole. The frequency content of the rotor response during run up and run down was analysed using the waterfall spectrum by extracting the frequency which produced the peak in the averaged lateral response. It was observed that the natural frequency dominates the response when the drillstring undergoes forward whirl with no contact with the borehole. However with continuous contact a jump in the frequency contents was observed. The jump in frequency content is observed when the rotor speed is near the lateral natural frequency. The frequency content is then dominated by the backward whirl frequency. A hysteresis in the jump behaviour of the system was observed with the backward whirl frequency dominating the response even at rotor speeds beyond the lateral resonance frequency during run down.

The study was extended to a multiple disc rotor to replicate the behaviour of a long drillstring with multiple stabilizers. The model incorporated the influence of axial loading due to self weight which can lead to the buckling of the drillstring. The axial loading changes from compression to tension along the drillstring. The axial loading induced a negative bending stiffness along the drillstring. A transition in behaviour at the stabilizer location was observed with continuous contact established along the drillstring at the stabilizer location depending on the excited mode.

The study indicates that the system parameters such as the eccentric mass position and phase, axial load and rotor speed are critical for the backward whirl behaviour. The two important parameters which are controllable while in operation are the rotor speed and the hook load. Hence during an actual drilling operation the backward whirl, which reduces the fatigue life of the drillstring, is influenced by the rotor speed and the axial hook load. A careful

tuning of these two parameters can control the mode excited and alter the backward whirl behaviour.

References

1. K. Vijayan and J. Woodhouse. Shock transmission in a coupled beam system. *Journal of Sound and Vibration*, 332(16):3681 – 3695, 2013.
2. K. Vijayan and J. Woodhouse. Shock amplification, curve veering and the role of damping. *Journal of Sound and Vibration*, 333(5):1379 – 1389, 2014.
3. S. Jardine, L. Malone, and M. Sheppard. Putting a damper on drilling’s bad vibrations. *Oil Field Review*, pages 15–20, 1994.
4. W.D. Aldred and M.C. Sheppard. Drillstring vibrations: a new generation mechanism and control strategies. In *SPE Annual Technical Conference and Exhibition*, 1992.
5. A. Muszynska, D. E. Bently, W. D. Franklin, J. W. Grant, and P. Goldman. Applications of sweep frequency rotating force perturbation methodology in rotating machinery for dynamic stiffness identification. *Journal of Engineering for Gas Turbines and Power-Transactions of the ASME*, 115(2):266–271, 1993.
6. P. Goldman and A. Muszynska. Chaotic behavior of rotor-stator systems with rubs. *Journal of Engineering for Gas Turbines and Power-Transactions of the ASME*, 116(3):692–701, 1994.
7. A. Muszynska and P. Goldman. Chaotic response of unbalanced rotor-bearing stator system with looseness or rubs. *Chaos Solitons & Fractals*, 5(9):1683–1704, 1995.
8. A. Muszynska. *Rotordynamics*. Taylor and Francis, 2005.
9. S. Edwards, A.W. Lees, and M.I. Friswell. The influence of torsion on rotor-stator contact in rotating machinery. *Journal of Sound and Vibration*, Vol. 225, No. 4:pp. 767–778, August 1999.
10. F. K. Choy and J. Padovan. Nonlinear transient analysis of rotor-casing rub events. *Journal of Sound and Vibration*, 113(3):529–545, 1987.
11. G. Genta. *Dynamics of rotating systems*. Springer, 2004.
12. M.I. Friswell, J.E.T. Penny, S.D. Garvey, and A.W. Lees. *Dynamics of Rotating Machines*. Cambridge University Press, 2010.
13. K. Vijayan. *Vibration and shock amplification of drilling tools*. PhD thesis, University of Cambridge, 2012.
14. H. H. Jeffcott. The lateral vibrations of loaded shafts in the neighbourhood of a whirling speed - the effect of want of balance. *Philosophical Magazine*, 37:304–314, 1919.
15. J. D. Jansen. Nonlinear rotor dynamics as applied to oilwell drillstring vibrations. *Journal of Sound and Vibration*, 147(1):115–135, 1991.
16. F. Chu and Z. Zhang. Bifurcation and chaos in a rub-impact jeffcott rotor system. *Journal of Sound and Vibration*, 210(1):1–18, 1998.

17. N. Mihajlovic, A. A. van Veggel, N. van de Wouw, and H. Nijmeijer. Analysis of friction-induced limit cycling in an experimental drill-string system. *Journal of Dynamic Systems Measurement and Control-Transactions of the Asme*, 126(4):709–720, 2004.
18. N. Mihajlovic, N. van de Wouw, M. P. M. Hendriks, and H. Nijmeijer. Friction-induced limit cycling in flexible rotor systems: An experimental drill-string set-up. *Nonlinear Dynamics*, 46(3):273–291, 2006.
19. N. Vljajic, X. Liu, H. Karkic, and B. Balachandran. Torsion oscillations of a rotor with continuous stator contact. *International Journal of Mechanical Sciences*, Vol. 83:pp.65–75, 2014.
20. C. M. Liao, N. Vljajic, H. Karki, and B. Balachandran. Parametric studies on drill-string motions. *International Journal of Mechanical Sciences*, 54(1):260 – 268, 2012.
21. V.I. Gulyayev and O.I. Borshch. Free vibrations of drill strings in hyper deep vertical bore-wells. *Journal of Petroleum Science and Engineering*, 78(3):759–764, 2011.
22. K Nandakumar and Marian Wiercigroch. Stability analysis of a state dependent delayed, coupled two dof model of drill-string vibration. *Journal of Sound and Vibration*, 332(10):2575–2592, 2013.
23. W. Weaver Jr, S. P. Timoshenko, and D. H. Young. *Vibration problems in engineering*. John Wiley & Sons, 1990.
24. M.P. Cartmell. *Introduction to linear, parametric and nonlinear vibrations*. Chapman and Hall London, 1990.

				Units
M_1	1	M_2	1	kg
m_1	0.05	m_2	0.05	kg
e_1	0.05	e_2	0.05	m
J_1	0.0025	J_2	0.0025	kg m ²
k_1	1	k_2	1	N/m
k_{t1}	0.5	k_{t2}	0	N/m
c_1	0.02	c_2	0.02	Ns/m
c_{t1}	1.83E-04	c_{t2}	1.83E-04	Ns/m
R_1	0.05	R_2	0.05	m
δ_1	0.01	δ_2	0.01	m
k_c	10			N/m
k_{tc}	0.5			N/m
c_s	0.1			Ns/m
k_s	10^5			N/m

Table 1: System parameters corresponding to the two disc model.

		ω_1	ω_2	ω_3	ω_4	ω_5	ω_6
Natural frequency (Hz)		0.16	0.16	0.71	0.71	1.36	3.42
	x_1	-0.71	0.00	0.00	-0.71	0.00	0.00
	x_2	-0.71	0.00	0.00	0.71	0.00	0.00
	y_1	0.00	-0.71	-0.71	0.00	0.00	0.00
	y_2	0.00	-0.71	0.71	0.00	0.00	0.00
	θ_1	0.00	0.00	0.00	0.00	-0.52	-0.85
	θ_2	0.00	0.00	0.00	0.00	-0.85	0.52

Table 2: Natural frequencies and mode shapes corresponding to the system parameters, without contact.

				Units
E_1	210×10^9	E_2	210×10^9	N/m^2
ρ_1	8050	ρ_2	4×8050	kg/m^3
e_1	0.05	e_2	0.05	m
d_o	0.2286	d_2	0.2286	m
d_i	0.0762	d_2	0.0381	m
G_1	77×10^9	G_{t2}	77×10^9	N/m
c_1	0.1	c_2	0.1	Ns/m
c_{t1}	0.08	c_{t2}	0.08	Ns/m
δ_1	0.01	δ_2	0.01	m
L_1	150	L_2	150	m
k_c	$10k_{1n}$			N/m
k_{tc}	k_t			N/m

Table 3: System parameters corresponding to the multiple discs model including drillstring and drillpipe.

Mode 1	
frequency	Eigenvector
0.12	0.95
	1
	0.85
	0.24
	0.1

Table 4: The natural frequency and mode shape corresponding to first mode for the multiple discs case.

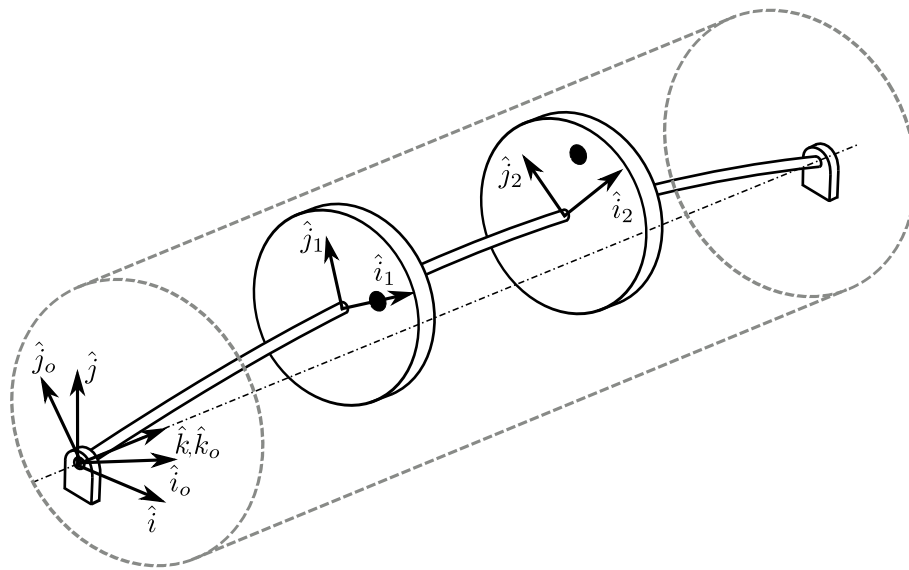


Fig. 1: Schematic of the two disc rotor model

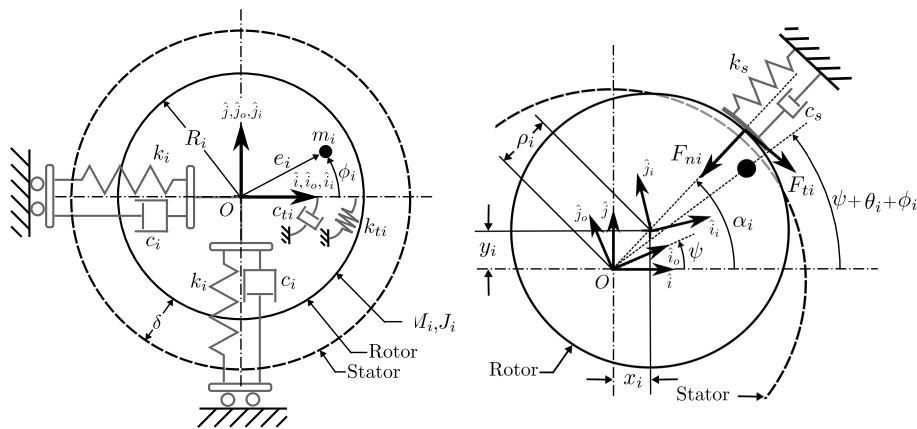


Fig. 2: Model of the two disc system including the contact model.

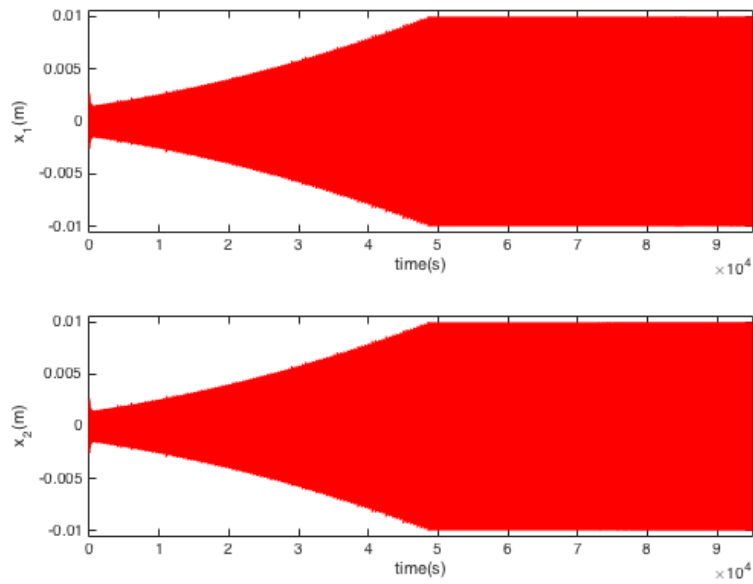
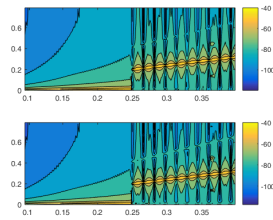
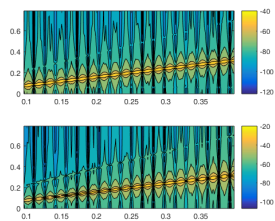


Fig. 3: Temporal variation in the lateral response of the two rotors during run up when the eccentric masses are in phase.



(a) Contour map of the waterfall spectrum during upsweep.



(b) Contour map of the waterfall spectrum during reverse sweep.

Fig. 4: The variation in frequency content of the response with change in rotor speed. A jump in frequency is observed near the first lateral mode.

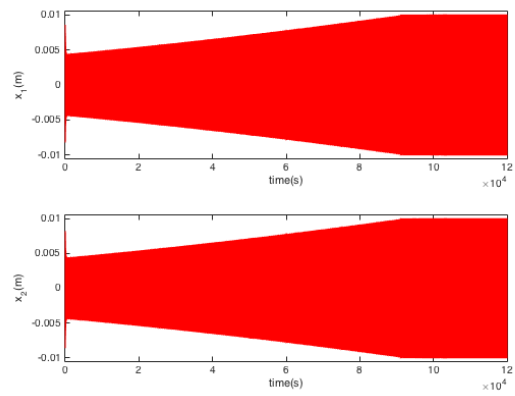
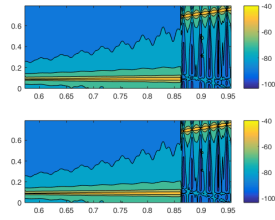
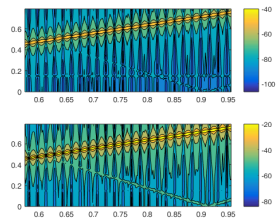


Fig. 5: Temporal variation in the normalised clearance during run up (red) and run down (green). The eccentric masses are out of phase.



(a) Contour map of the waterfall spectrum during upsweep.



(b) Contour map of the waterfall spectrum during reverse sweep.

Fig. 6: The variation in frequency content of the response with change in rotor speed. A jump in frequency is observed near the second lateral mode.

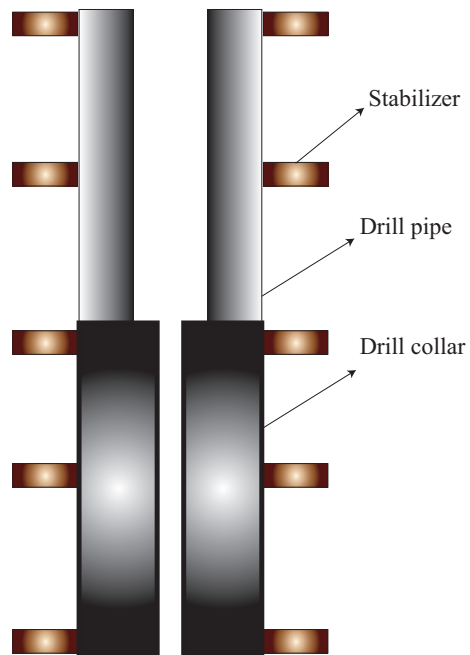


Fig. 7: Drillstring system comprising of drill pipe and drill collar with stabilizers. The drill collar is heavier than the drill pipe.

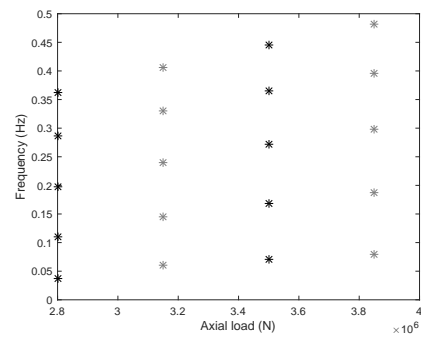


Fig. 8: Variation of first five bending natural frequencies for different hook loads.

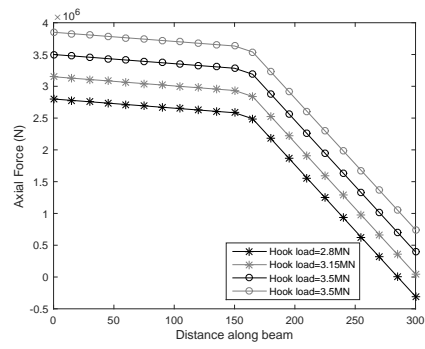


Fig. 9: Variation in axial force along the drillstring corresponding to different hook load.

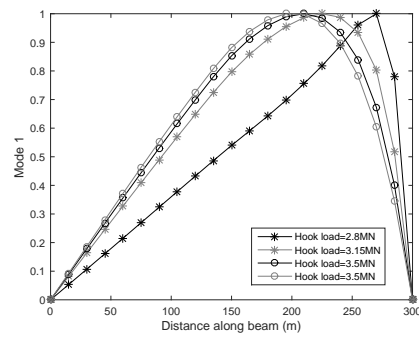


Fig. 10: Variation in the mode shape of the first mode (buckling mode) for different hook loads.

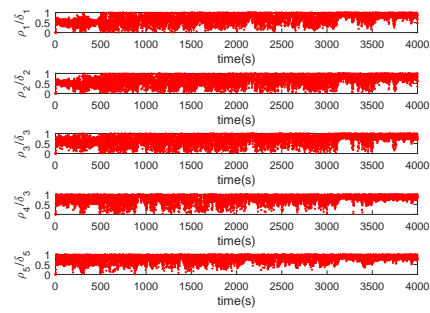


Fig. 11: Variation in the response of the system, normalised with respect to clearance. Rotor speed was swept (ω_e) from 0.005 to 0.04 Hz. The initial position and phase of the eccentric mass was tuned to excite the first mode of the system.